Journal of Inorganic Biochemistry 201 (2019) 110815

Contents lists available at ScienceDirect

Journal of Inorganic Biochemistry

journal homepage: www.elsevier.com/locate/jinorgbio

Vanadium(V) tris-3,5-di-*tert*-butylcatecholato complex: Links between speciation and anti-proliferative activity in human pancreatic cancer cells

Edie Griffin[a], Aviva Levina[a,*], Peter A. Lay[a,b,*]

[a] School of Chemistry, University of Sydney, Sydney, NSW 2006, Australia
[b] Sydney Analytical, University of Sydney, Sydney, NSW 2006, Australia

ARTICLE INFO

Keywords:
Vanadium
Pancreatic cancer
Speciation
Cytotoxicity
Human serum albumin
Intratumoral injections

ABSTRACT

Vanadium complexes are intensively tested for anti-cancer activities, particularly for the novel treatment protocols involving injections of cytotoxic compounds directly into the tumor. This approach is increasingly applied to difficult-to-treat cancers, such as pancreatic cancer. The first study of in-vitro anti-cancer properties of a rare stable non-oxido V(V) complex, $(NH_4)[V(dtbc)_3]$, where $dtbcH_2$ is 3,5-di-*tert*-butylcatechol, was performed by a combination of end-point viability assays and real-time (IncuCyte) proliferation and cytotoxicity assays in human pancreatic cancer (PANC-1) cells. An improved synthetic procedure led to a nearly quantitative yield of the complex under ambient conditions. Reactions of $(NH_4)[V(dtbc)_3]$ either in polar organic solvents or in neutral aqueous media led to the formation of V(V)-oxido-catecholato intermediates (characterized by electrospray mass spectrometry) that were responsible for its anti-proliferative and cytotoxic (apoptotic or necrotic) activity (IC_{50}, 3.5–18 μM V in 72 h assays). These results demonstrate the link between solution speciation and biological activity of V complexes. Reaction of $(NH_4)[V(dtbc)_3]$ with human serum albumin (HSA) in aqueous media led to the formation of protein-bound V(V) oxido-catecholato species that showed high anti-proliferative activity (IC_{50} ~10 μM V) combined with low cytotoxicity. Formation of HSA adducts of hydrophobic V complexes, such as $(NH_4)[V(dtbc)_3]$, is a promising way to achieve their sustained delivery to cancer tumors.

1. Introduction

Diverse biological activities of V(IV) and V(V) complexes, particularly their anti-diabetic and anti-cancer (including anti-mutagenic [1]) properties, have been actively studied over the last three decades [2–6]. Pancreatic cancer is one of the most difficult cancers to treat [7,8], and there is considerable interest in developing new pancreas-specific chemotherapeutic agents, including V complexes [9,10]. The main problem that has hampered the introduction of V-based drugs into clinical practice is the complicated ligand-exchange and redox chemistry of V under biologically-relevant conditions [11–13], which leads to low stability of typical medicinal V complexes in biological media [14,15] and their unpredictable pharmacokinetics [16–19]. Recently, the Crans and Lay groups have suggested that the low stability of V complexes in biological media can be turned into advantage for the use in intratumoral injections for difficult-to-treat cancers, including pancreatic cancer [7,8]. Namely, a V(V) monooxido complex that contained a tridentate Schiff base (*N*-(salicylideneaminato)-*N*′-(2-hydroxyethyl) ethane-1,2-diamine) and a bidentate 3,5-di-*tert*-butylcatecholato ligand (**1** in Chart 1) [20,21] survived long enough in cell culture medium to enter cultured human cancer cells intact and cause high cytotoxicity, while its decomposition products in the medium were less toxic [21], which is expected to reduce the systemic toxicity of **1** after its release into the blood stream (A. Levina, D. C. Crans, P. A. Lay et al., manuscript in preparation). The enhanced stability of **1** in biological media was due to the steric hindrance of ^{t}Bu groups, since the same complex with unsubstituted catechol decomposed within seconds under the conditions of cell assays [21]. Notably, a tris-catecholato V(V) complex, $[V(dtbc)_3]^-$ ((where dtbc = 3,5-di-*tert*-butylcatecholato(2-)); **2** in Chart 1) formed during the decomposition of **1** in neutral aqueous solutions (identified by mass spectrometry and electronic absorption spectroscopy) [22] and persisted longer than **1** under these conditions (A. Levina, unpublished observation).

Compound **2** was probably the first isolated non-oxido V(V) complex [23], characterized by X-ray crystallography in 1986 [24]. Although non-oxido V(V) complexes are rare [25,26], they came into prominence recently, particularly as catalytic intermediates in water oxidation catalyzed by amavadin (a natural non-oxido V(IV) complex) and its synthetic analogues [27]. Detailed experimental (X-ray absorption spectroscopy) and computational studies of charge distribution

* Corresponding authors.
E-mail addresses: aviva.levina@sydney.edu.au (A. Levina), peter.lay@sydney.edu.au (P.A. Lay).

https://doi.org/10.1016/j.jinorgbio.2019.110815
Received 2 May 2019; Received in revised form 26 August 2019; Accepted 31 August 2019
Available online 03 September 2019
0162-0134/

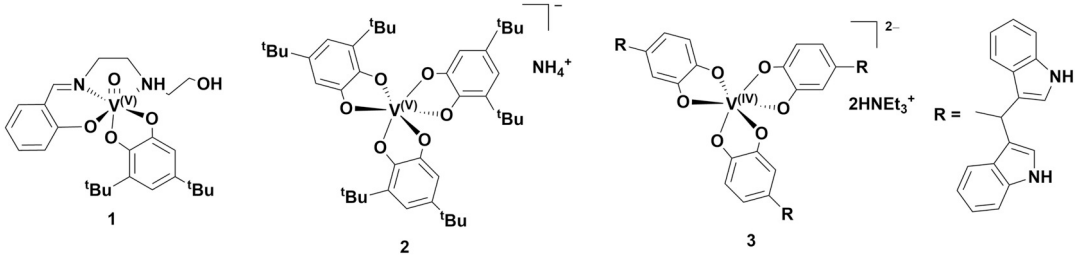

Chart 1. Typical structures of V-catecholato complexes with in vitro anti-cancer activities: a Schiff base-catecholato-oxido V(V) complex **1** [20,21]; a tris-catecholato V(V) complex **2** (studied in this work) [22–24]; and a tris-catecholato V(IV) complex **3** [31].

between V(V) center and the ligands in **2** have been performed by our group [22]. Complex **2** is among the intermediates that are likely to form during V(V)-catalyzed oxidation of 3,5-di-*tert*-butylcatechol by O_2 (a model of catechol dioxygenase enzymes) [28,29]. Insulin-mimetic activity of a related complex, $[V^{IV}(cat)_3]^{2-}$ (where cat = catecholato(2-)), in cell culture systems was linked to its hydrolysis and oxidation with the formation of V(IV) and V(V) oxido species [30]. To our knowledge, the anti-cancer activity of **2** has not been studied previously [15], although encouraging results have been obtained for a non-oxido V(IV) complex with catechol-modified 3,3′-diindolylmethane (**3** in Chart 1) [31] and for V(IV)-oxido-catecholato complexes with flavonoid ligands [32,33]. In this work, we present an improved synthetic method for **2** and a detailed study of its reactivity under cell culture conditions, in conjunction with proliferation and cytotoxicity assays in human pancreatic cancer (PANC-1) cells. Formation of an adduct of **2** with human serum albumin (HSA) is proposed as a convenient way of delivery of cytotoxic V(V) to pancreatic tumors.

2. Experimental

2.1. Materials

Analytical grade (> 99% purity) reagents and HPLC grade solvents from Sigma-Aldrich or Merck were used without further purification, and water was purified by the Milli-Q technique. Trace pure HNO_3 (69% w/v in H_2O) and HCl (37% w/v in H_2O) from Merck were used for digestion of samples for V determination by graphite furnace atomic absorption spectrometry (GFAAS), and certified V standard solution (Aldrich 18399) was used for GFAAS calibration. Human serum albumin (Sigma A3782) was used for the preparation of adduct with **2**. Pre-sterilized media and sterile plasticware used in cell culture were purchased from Life Technologies Australia. PANC-1 (epithelioid carcinoma of the pancreas) cells were purchased from American Type Culture Collection (ATCC, Cat. No. CRL-1469).

2.2. Instrumentation and software

Solution NMR spectra were recorded at 300 K on a Bruker Avance 400 MHz spectrometer. ^{51}V NMR spectra were collected at 26.35 MHz [34] in the −1000 to 500 ppm spectral window (2560 scans; total scan time, 23 min), and were externally referenced using 100 mM Na_3VO_4 solution in 1.0 M NaOH ($[VO_4]^{3-}$ signal at −541 ppm) [34]. ^1H NMR spectra were collected in the −10 to 15 ppm spectral window (16 scans, 2 min) and were internally referenced to the solvent peak (d_6-DMSO, 2.50 ppm, where DMSO is dimethyl sulfoxide) [35]. Determinations of V content in solid **2**, **2**-HSA adduct and cell culture media were performed on an Agilent Technologies series 200 GFAAS spectrometer, equipped with Zeeman background correction.

Low resolution electrospray ionization mass spectrometry (ESI-MS) data were collected on a Bruker amaZon SL spectrometer, using the following parameters: nebulizer pressure, 27.3 psi; spray voltage, 4.5 kV; capillary temperature, 453 K; N_2 flow rate, 4 L min^{-1}; *m/z* range, 100–1000 (alternating positive- and negative-ion modes). Analyzed solutions (5.0 μL) were injected into a flow of MeOH (flow rate, 0.30 mL min^{-1}). Acquired spectra were the averages of 100–200 scans (scan time, 10 ms). Simulations of the mass spectra were performed using IsoPro software [36]. High resolution negative ion ESI-MS was performed on a Bruker Solarix 2XR 7 T Fourier transform ion cyclotron resonance mass spectrometer via syringe infusion at 120 μL per hour. The transient length was 2M and acquired in 2-ω mode and the Fourier transform was performed in adsorption mode. The instrument was externally calibrated from 300 to 2000 *m/z* prior to analysis, and the isotopic patterns were simulated using Bruker Compass Data Analysis 5.0 software. Elemental (C, H, N) analysis were performed by the microanalytical services of Macquarie University (Sydney, Australia) and University of Otago (New Zealand).

Solution X-band (9.66 GHz) EPR spectra of decomposition products of **2** (10 mM in DMF, where DMF is *N*,*N*-dimethylformamide) or of a reference V(IV) compound, $VOSO_4{\cdot}5H_2O$ (10 mM in H_2O) were collected at 295 K using a Bruker EMX Nano spectrometer, equipped with internal NMR gaussmeter and microwave frequency meter. Solutions were placed inside glass capillaries (length, 10 mm, internal diameter, 1 mm), using a Hamilton syringe. The capillaries were sealed from the top with vacuum grease and placed inside a quartz EPR tube (Bruker). The spectra were acquired at 3480 G center field; 2000 G sweep width, 2.5 mW microwave power, 100 kHz modulation frequency, 5.0 G modulation amplitude, and 60 s scan time.

Electronic absorption (UV–vis) spectra were collected on a Hewlett-Packard HP 8452 A diode-array spectrometer (λ = 300–820 nm; resolution, 2 nm; integration time, 0.20 s), equipped with HP89090A Peltier temperature controller. Circular dichroism (CD) spectra were collected on a Jasco 710 spectropolarimeter (spectral range, 300–800 nm; resolution, 1.0 nm, integration time, 0.25 s; average of 20 scans). The pH values of aqueous solutions were checked immediately before use with Activon 210 ionometer that was equipped with AEP 321 glass/Ag/AgCl electrode and calibrated daily using standard pH solutions (Aldrich).

Real-time cell proliferation and cytotoxicity data were collected using Essen Bioscience IncuCyte Zoom imaging system [37] that was placed inside a cell culture incubator (310 K, 5% CO_2). For all IncuCyte experiments, images were collected every 2 h for 96 h, using ×10 objective. Green and red fluorescence acquisition times were 0.40 s and 0.80 s, respectively. Image analyses were performed with IncuCyte software [37], using the following parameters: cell over background threshold, 1.0; minimal object size, 300 μm^2; green threshold, 2.0; red threshold, 0.5; 5% of green fluorescence removed from the red channel. Absorbance measurements at 450 nm for WST-8 cell viability assays [38] were performed on a Victor V^3 multi-well plate reader. Plotting and statistical analysis of cell culture assay results were performed using Origin software [39].

2.3. Synthesis and characterization of 2

The complex was synthesized by a modified literature procedure [23]. Ammonium metavanadate (NH_4VO_3, 50 mg, 0.42 mmol) and 3,5-di-*tert*-butylcatechol ($dtbcH_2$, 285 mg, 1.28 mmol) were dissolved in

HPLC grade acetonitrile (MeCN, 12 mL), and the solution was stirred for 20 h at 295 K under ambient air atmosphere. The resultant dark blue precipitate was separated by vacuum filtration, washed with cold MeCN, and dried under vacuum over silica gel for 48 h at 295 K. Yield, 279 mg (91%). Vanadium content (GFAAS): (7.1 ± 0.2)% mass. (n = 3), calc. 7.00%. ^{1}H NMR (10 mM in d_6-DMSO): δ 1.18 and 1.22 (s, ^{t}Bu groups, 18H); δ 6.15 and 6.44 (s, Ph ring, 2H). ^{51}V NMR (10 mM in d_6-DMSO): δ −255. High resolution ESI-MS (~50 μM in MeCN): m/z = −711.38387 (calculated for $C_{42}H_{60}O_6V$, 711.38350). UV–vis (50 μM in DMF): λ_{max} = 630 nm, $\varepsilon_{max} = 1.4 \times 10^4\ M^{-1}\ cm^{-1}$ (Lit. $14.7 \times 10^3\ M^{-1}\ cm^{-1}$ at 630 nm in MeCN) [22].

2.4. Isolation and characterization of human serum albumin (HSA) adduct of 2

A solution of 50 mg HSA (MW = 66 kDa, 0.757 μmol) in Milli-Q H_2O (0.80 mL) was mixed with a solution of **2** (0.89 mg, MW = 729 Da, 1.22 μmol V) in DMSO (0.12 mL). The resultant dark blue solution was immediately loaded on a 3 kDa membrane filter (Pall Life Sciences) and centrifuged at 14,000*g* for 15 min at 277 K, to remove low molecular mass components. The residue on the filter was washed with Milli-Q H_2O (1.0 mL; 14,000*g* for 15 min at 277 K), then dissolved in ~0.10 mL H_2O and freeze-dried (217 K and 0.5 mbar for 16 h). The resultant blue solid was stored desiccated over silica gel at 277 K. For the determination of V content, three aliquots of the freeze-dried sample (~1.0 mg, weighed with 0.01 mg precision) were digested with trace pure HNO_3 (69% w/v; 0.20 mL) and diluted with 0.10 M HCl (trace pure) to ~10 μM V for GFAAS analysis. The V content (24 ± 2 nmol V per mg protein) corresponded to quantitative V-protein binding. UV–vis (0.24 mM V in H_2O): λ_{max} = 660 nm; $\varepsilon_{max} = 2.1 \times 10^3\ M^{-1}\ cm^{-1}$.

2.5. Cell culture, proliferation and cytotoxicity assays

The PANC-1 cells were cultured using standard techniques [40] in Advanced DMEM (Thermo Fisher 12491-015; DMEM is Dulbecco's modified Eagle's minimal essential medium), supplemented with L-glutamine (2.0 mM), antibiotic-antimycotic mixture (100 U mL^{-1} penicillin, 100 mg mL^{-1} streptomycin and 0.25 mg mL^{-1} amphotericin B) and foetal calf serum (FCS; heat-inactivated; 2% vol). For proliferation and cytotoxicity experiments, cells were seeded in 96-well plates at an initial density of (1–2) × 10^3 viable cells per well in 100 μL medium and left to attach overnight.

Stock solutions of **2** (10 mM in DMF) were either prepared on the day of experiments (fresh solutions) or stored for two weeks at 295 K prior to the experiments (aged solutions, see Results). Stock solutions of Na_3VO_4 (10 mM in H_2O) or $dtbcH_2$ (30 mM in DMF) were prepared on the day of experiments. Solutions of **2**-HSA adduct were prepared by dissolving the solid in fully supplemented cell culture medium, which was then sterilized by membrane filtration (0.20 μM pore size). Stock solutions of the treatment compounds were diluted with fully supplemented cell culture media to the required final concentrations, and the resultant media were either added to the cells within 1 min (fresh solutions), or left in cell culture incubator (310 K, 5% CO_2) for 24 h prior to the cell treatments (equilibrated solutions). Concentrations of V in cell culture media were verified by GFAAS and were within 10% of the expected values. Each treatment included six replicate wells and two background wells that contained the same components except the cells.

For endpoint assays, the plates were incubated for 72 h at 310 K and 5% CO_2, then WST-8 reagent [38] (10 μL per well) was added, and incubation was continued for 6 h, followed by absorbance measurements at 450 nm. Typically, the treatment compounds were applied in a series of five two-fold dilutions, starting from 80 μM V, plus the vehicle control, and the IC_{50} values were calculated using Origin software [39]. Similar techniques were used for real-time (IncuCyte Zoom) proliferation assays, but the treatment compounds (fresh or pre-equilibrated with the medium) were applied at 10 μM V concentrations. Real-time cytotoxicity (apoptosis and cell death) was followed by IncuCyte Zoom in the presence of Caspase 3/7 Green (3.0 μM) [41] and Cytotox Red (0.30 μM) [42] fluorescent dyes that were added to cell culture medium immediately before the measurements.

For all the cell assays, consistent results were obtained in at least two independent experiments, using different passages of cells and different stock solutions of the treatment compounds.

3. Results and discussion

3.1. Synthesis and characterization of 2

The first reported synthesis of $[V(dtbc)_3]^-$ by the reaction of NH_4VO_3 with excess $dtbcH_2$ in MeOH/Et_3N led to a low yield of the product (16%) [23]. Subsequently, $[V(dtbc)_3]^-$ was synthesized either by the reaction of $[V(CO)_6]^-$ with 3,5-di-*tert*-butyl-1,2-benzoquinone (dtbq) [24], or by the reaction of $[VO(acac)_2]$ (acac = 2,4-pentanedionato(−)) with $dtbcH_2$ in the presence of Et_3N [22]. Both reactions required the use of dry solvents and inert atmosphere. By contrast, we found that the reaction of NH_4VO_3 with three molar equivalents of $dtbcH_2$ in MeCN under ambient conditions led to precipitation of $(NH_4)[V(dtbc)_3]$ (**2**, dark blue solid) [22–24] with near-quantitative yield (Eq. (1), see Experimental for details):

$$NH_4VO_3 + 3\ dtbcH_2 \rightarrow (NH_4)[V(dtbc)_3] + 3\ H_2O\ (MeCN, 20\ h\ at\ 295\ K). \quad (1)$$

^{1}H NMR spectroscopic data on **2** (10 mM in d_6-DMSO; Fig. 1a–c) showed neat replacement of the signals of aromatic and aliphatic (^{t}Bu groups) protons of the ligands with the corresponding signals due to the V(V) complex. While the single set of both the ^{t}Bu and aromatic proton signals are indicative of a pure *fac* isomer in solution, they are broader in the complex than the free ligand, which may be indicative of an equilibrium between the *fac* and *mer* isomers that isomerize on a comparable timescale as the NMR timescale. Broadening due to coupling with ^{51}V nucleus would be expected to be different for the different proton environments, which does not appear to be the case, but variable temperature NMR would be required to detect the presence of isomers. ^{51}V NMR spectroscopic data from the same solution (Fig. 1d) showed the main signal at −255 ppm, which was consistent with V(V) tris-catecholato complexes [43], and an additional signal at −510 ppm, which was due to V(V) oxido-catecholato species (a mixture of *cis* and *trans* isomers is likely) [34] that are formed during the reactions of **2** with trace H_2O and O_2 in d_6-DMSO solutions (see below). Close inspection of the ^{51}V NMR signal at −255 ppm showed that there were two peaks (inset in Fig. 1d), which was consistent with both the *fac* and *mer* isomer being present in solution. Low resolution ESI-MS data for a freshly prepared solution of **2** (50 μM in DMF/MeOH; Fig. 2a, b and Table 1) showed a clean signal of the parent complex ($[V(dtbc)_3]^-$, m/z = −711) [22] in the negative mode, as well as its Na^+ adducts and a trace of oxidized ligand (dtbq) in the positive mode. The identity of the m/z = −711 signal has been confirmed by high-resolution ESI-MS (Fig. S1 in Supplementary Information). Electronic absorption (UV–vis) spectroscopy of the same solution showed a strong signal at λ_{max} = 630 nm, $\varepsilon_{max} = 1.4 \times 10^4\ M^{-1}\ cm^{-1}$ (line (1) in Fig. 3a), which is consistent with literature data for $[V(dtbc)_3]^-$ [22,23]. Repeated C, H, N analyses of the solid **2** resulted in significantly lower than expected C content, possibly due to the formation of V carbides during the thermal decomposition of the complex [44].

3.2. Reactivity of 2 in organic solvents and in neutral aqueous solutions

ESI-MS data for **2** under biomimetic conditions of pH and concentrations (50 μM V in 10 mM aqueous NH_4HCO_3/MeOH, pH 7.5) [45] showed significant hydrolysis of $[V(dtbc)_3]^-$ within 30 min at 295 K with the release of free ligand and the formation of $[VO(dtbc)_2]^-$ (Fig. 2c, d and Table 1). The corresponding UV–vis spectrum (line (2) in

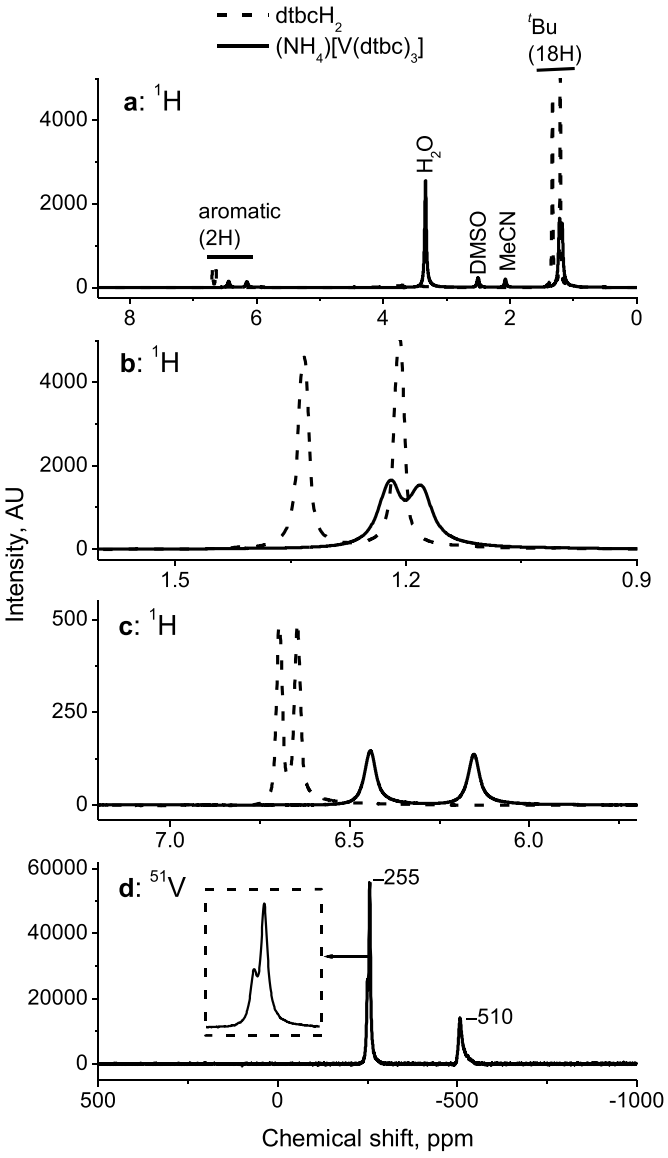

Fig. 1. Comparison of NMR spectra of $(NH_4)[V(dtbc)_3]$ (**2**) and the free ligand (fresh solutions in d_6-DMSO; 10 mM **2** or 30 mM $dtbcH_2$): (a) overview of ^1H NMR spectra; (b) protons of the ^{t}Bu groups; (c) protons of the phenyl rings; and (d) ^{51}V NMR spectrum of **2**. Solvent peaks in (a) were assigned according to literature data [35].

Fig. 3a) was consistent with the presence of a mixture of $[V(dtbc)_3]^-$ and hydrolysis products. Aqueous solutions used in Fig. 2c, d were obtained by dilution of freshly prepared stock solution of **2** in DMF (10 mM, dark-blue). If this solution was left to stand under ambient atmosphere at 295 K, its color gradually changed from blue to green to yellow within two weeks (Fig. S2 in Supplementary Information). Similar time-dependent spectral changes occurred for a 10 mM solution of **2** in DMSO (Fig. S2). ESI-MS of an aged (two weeks at 295 K) solution of **2** in DMF, diluted with MeOH to 50 μM V (Fig. 2e, f and Table 1), showed the formation of V(V) oxido-catecholato complexes ($[VO(dtbc)_2]^-$ and $[VO(dtbc)(OMe)_2]^-$), as well as of the oxidized ligand (dtbq). These changes corresponded to the formation of an absorbance band at λ_{max} = 390 nm in UV–vis spectra (line (3) in Fig. 3a). Similar reactions occurred during the V(V)-catalyzed oxidation of $dtbcH_2$ by O_2 in organic solvents [28,29]. No detectable amounts of V(IV) species [46] or semiquinone radicals [28] were observed in decomposed solution of **2** (10 mM in DMF) by EPR spectroscopy (Fig. S3 in Supplementary Information).

3.3. Characterization of *2*-HSA adduct

Reaction of a concentrated aqueous solution of HSA with 1.6 molar equivalents of **2** resulted in quantitative V binding to the protein (see Experimental for details). The blue color of the freeze-dried adduct and its V content (determined by GFAAS) did not change for at least six months when stored desiccated at 277 K. A concentrated solution of the **2**-HSA adduct (10 mg mL^{-1} protein, 0.24 mM V) in phosphate buffered saline (PBS; 150 mM NaCl, 20 mM phosphate, pH 7.4) showed characteristic absorbance of V-catecholato complexes at λ_{max} ~660 nm (line (1) in Fig. 3b), but its intensity was ~15% of that for the fresh solutions of **2** in organic solvents ($\varepsilon_{max} = 2.1 \times 10^3\ M^{-1}\ cm^{-1}$). These data suggest that $[V(dtbc)_3]^-$ was partially hydrolyzed during isolation of the HSA adduct and/or during its re-dissolution in PBS. The same solution showed a weak but significant CD signal at ~650 nm (line (2) in Fig. 3b), which confirms that V-dtbc species interacted with the chiral environment of HSA. A weak CD signal (Fig. 3b) is consistent with predominantly non-covalent **2**-HSA binding, most likely due to the

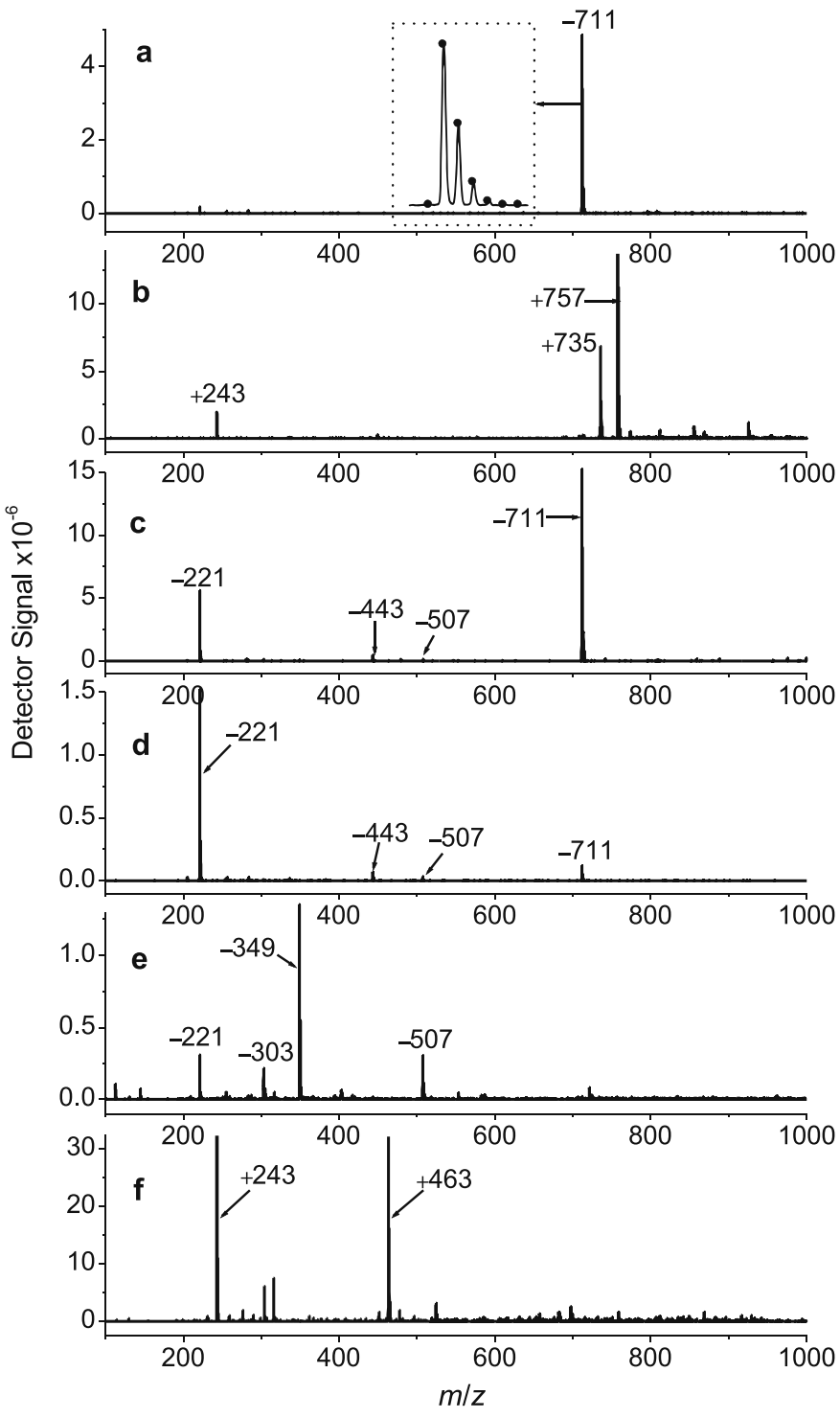

Fig. 2. Typical low-resolution ESI-MS data for **2** and its decomposition products (see Table 1 for assignment of the major signals and Fig. S1 for high-resolution data). Reaction conditions: (a) freshly prepared 10 mM **2** in DMF, diluted 200-fold with MeOH, negative ion mode; (b) same as (a), positive ion mode; (c) freshly prepared 10 mM **2** in DMF, diluted 100-fold with 10 mM aqueous NH_4HCO_3 (pH ~7.5), then immediately diluted 2-fold with MeOH, negative ion mode; (d) freshly prepared 10 mM **2** in DMF, diluted 100-fold with 10 mM aqueous NH_4HCO_3 (pH ~7.5), reacted for 30 min at 295 K, then diluted 2-fold with MeOH, negative ion mode; (e) 10 mM **2** in DMF, aged for 14 days at 295 K, then diluted 200-fold with MeOH, negative ion mode; (f) same as (e), positive ion mode. The inset in (a) shows experimental (line) and simulated [36] (dots) isotopic distribution for the main signal.

interactions of lipophilic dtbc ligands with the hydrophobic binding pockets of HSA [47,48].

3.4. Effects of 2, 2-HSA and their decomposition products on PANC-1 cell viability

Conditions for testing the anti-proliferative activity of **2** in PANC-1 cells (Table 2) were designed based on its reactivity studies in organic solvents (used for preparation of stock solution for cell assays) [14] and in neutral aqueous media (Figs. 2 and 3). Like our studies with other V complexes [21,45], the effect of **2** that was freshly added to cell culture medium was compared with that of **2** equilibrated with cell culture medium for 24 h at 310 K and 5% CO_2 before the addition to cells (conditions 2 and 3 in Table 2). Equilibration conditions were chosen based on the results of X-ray absorption spectroscopic studies of typical biologically relevant V(V) and V(IV) complexes [49], which showed their convergence into the same mixtures of predominantly five-coordinate V(V) (~75%) and six-coordinate V(IV) species under these conditions. Studies on **2** that was aged in DMF stock solution for two weeks prior to the addition to cell culture medium were also performed (conditions 4 and 5 in Table 2), since such aging significantly changed V speciation (Figs. 2e, f and 3a). Dissolution of the solid **2**-HSA adduct

Table 1
Assignment of ESI-MS signals (Fig. 2).

m/z[a]	Assignment[b]
−221	$dtbcH^-$
+243	$dtbq{\cdot}Na^+$
−303	$[V(O)_2(dtbc)]^-$
−349	$[VO(dtbc)(OMe)_2]^-$
−443	$dtbcH_2{\cdot}dtbcH^-$
+463	$2dtbq{\cdot}Na^+$
−507	$[VO(dtbc)_2]^-$
−711	$[V(dtbc)_3]^-$
+735	$[V(dtbc)_3]^-{\cdot}H^+{\cdot}Na^+$
+757	$[V(dtbc)_3]^-{\cdot}2Na^+$

[a] The *m/z* values correspond to the most abundant peaks in the isotope distribution (Fig. 2). ESI-MS conditions are listed in the Experimental Section.

[b] Designations: $dtbcH_2$ = 3,5-di-*tert*-butylcatechol; dtbq = 3,5-di-*tert*-butyl-1,2-benzoquinone.

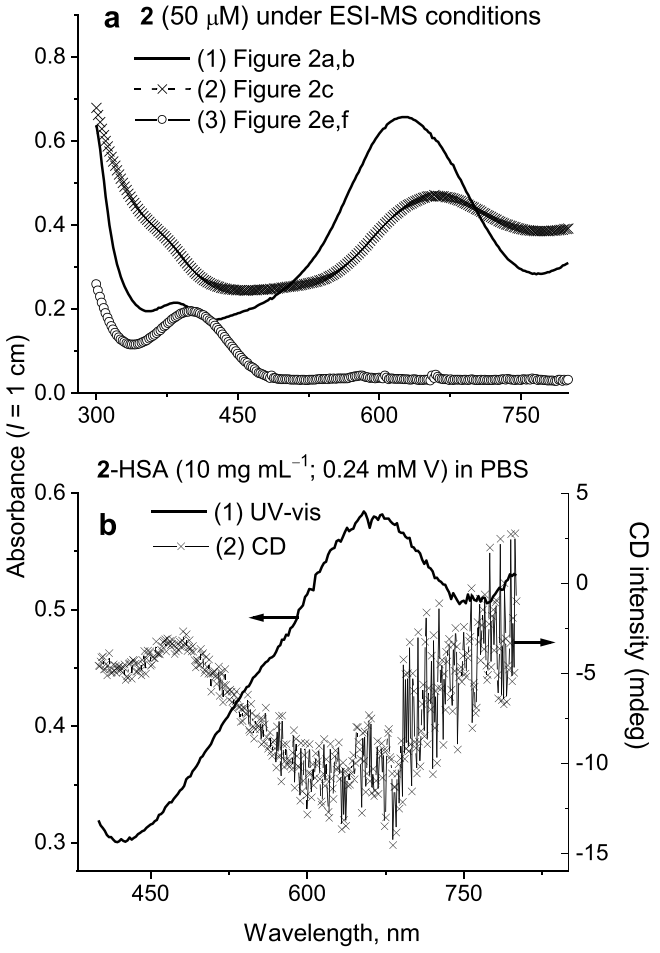

Fig. 3. Typical electronic absorption (UV–vis) and circular dichroism (CD) spectra for **2** and its decomposition products at 295 K: (a) UV–vis spectra of dilute solutions of **2** (50 μM), prepared identically to those used in ESI-MS (Fig. 2 and Table 1); and (b) UV–vis (line (1)) and CD (line (2)) of a freshly prepared concentrated solution of **2**-HSA adduct in PBS. The CD spectrum (average of 20 scans) was normalized against a spectrum of PBS blank, recorded under identical conditions.

in cell culture medium either immediately or 24 h before the cell treatment (conditions 6 and 7 in Table 2) was studied as an alternative to using stock solutions of **2** in organic solvents. Separate addition of V (V) (Na_3VO_4) and $dtbcH_2$ (three molar equivalents to V), followed by 24 h equilibration, was used to model the decomposition products of **2**

Table 2
Conditions of cell viability assays for **2** and its decomposition products in PANC-1 cells.

Cond.[a]	Reagent	Medium[b]	IC_{50}, μM[c]
1	Vehicle control[d]	Fresh	–
2	**2**, fresh stock[e]	Fresh	18 ± 4
3	**2**, fresh stock[e]	Equil.	17 ± 4
4	**2**, aged stock[f]	Fresh	(3.5 ± 0.8)***
5	**2**, aged stock[f]	Equil.	16 ± 4
6	**2**-HSA[g]	Fresh	(9.5 ± 2.5)*
7	**2**-HSA[g]	Equil.	17 ± 4
8	Na_3VO_4[h] + 3 eq. $dtbcH_2$[i]	Equil.	15 ± 3
9	Na_3VO_4[h]	Equil.	(26 ± 5)*
10	$dtbcH_2$[i]	Equil.	(66 ± 11)***

[a] Designations of experimental conditions correspond to those used in Figs. 4–6 and S4–S7.

[b] Mode of addition of the reagents to cell culture medium: Fresh = freshly added to the medium (within 1 min before treating the cells); Equil. = pre-equilibrated with cell culture medium for 24 h at 310 K and 5% CO_2 before treating the cells.

[c] Concentration of the treatment (μM) that caused 50% decrease in cell viability after 72 h treatment (determined by WST-8 colorimetric assay; see Fig. S4 for details) [38]. The data are the mean values and standard deviations of six replicate wells. One or three stars designate statistically significant differences ($P < 0.05$ or $P < 0.001$, respectively; one-way ANOVA) [39] compared with condition 2.

[d] DMF (0.20% vol.) in cell culture medium; the same amount of DMF was present under all the experimental conditions.

[e] Stock solution (10 mM V in DMF) was prepared within 1 h before the addition to cell culture medium and had dark blue color (λ_{max} = 630 nm, line (1) in Fig. 3a).

[f] Stock solution (10 mM V in DMF) was kept for two weeks at 295 K before the addition to cell culture medium and had yellow-green color (λ_{max} = 390 nm, line (3) in Fig. 3a).

[g] Isolated solid (see Experimental Section) was directly dissolved in cell culture medium, followed by sterile filtration; DMF (0.20% vol) was added separately to cell culture medium.

[h] Stock solution (10 mM V in sterile H_2O) was prepared on the day of the experiment; DMF (0.20% vol) was added separately to cell culture medium.

[i] Stock solution of $dtbcH_2$ (30 mM in DMF) was prepared on the day of the experiment.

in cell culture medium (condition 8 in Table 2) [14,15]. For comparison, either Na_3VO_4 or $dtbcH_2$ were added alone and equilibrated with cell culture medium (conditions 9 and 10 in Table 2). All the conditions (Table 2) included the same amount of organic solvent (0.20% vol. DMF), which did not have a significant effect at cell growth at this concentration [50].

Concentration-dependent changes in the PANC-1 cell viability under the conditions listed in Table 2 (72 h incubation, WST-8 colorimetric assay) [38] are shown in Fig. S4, Supplementary Information, and the corresponding IC_{50} values are listed in Table 2. Most notably, aging of **2** in DMF solution led to five-fold increase in anti-proliferative activity compared with a fresh solution of **2** in DMF, when both solutions were freshly added to cell culture medium (conditions 2 and 4 in Table 2). There was also nearly two-fold increase in activity for **2**-HSA that was freshly dissolved in cell culture medium, compared with freshly added solution of **2** in DMF (conditions 2 and 6 in Table 2). There was no significant difference in activity of V-containing treatments that were equilibrated with cell culture medium (conditions 3, 5, 7 and 8 in Table 1), except for a slightly lower effect of Na_3VO_4 alone (condition 9 in Table 2). By contrast, the ligand alone had much lower activity (condition 10 in Table 2). Based on the IC_{50} values listed in Table 2, 10 μM V and/or 30 μM $dtbcH_2$ were used for more detailed studies of anti-proliferative activities of **2** and its decomposition products (see next sections).

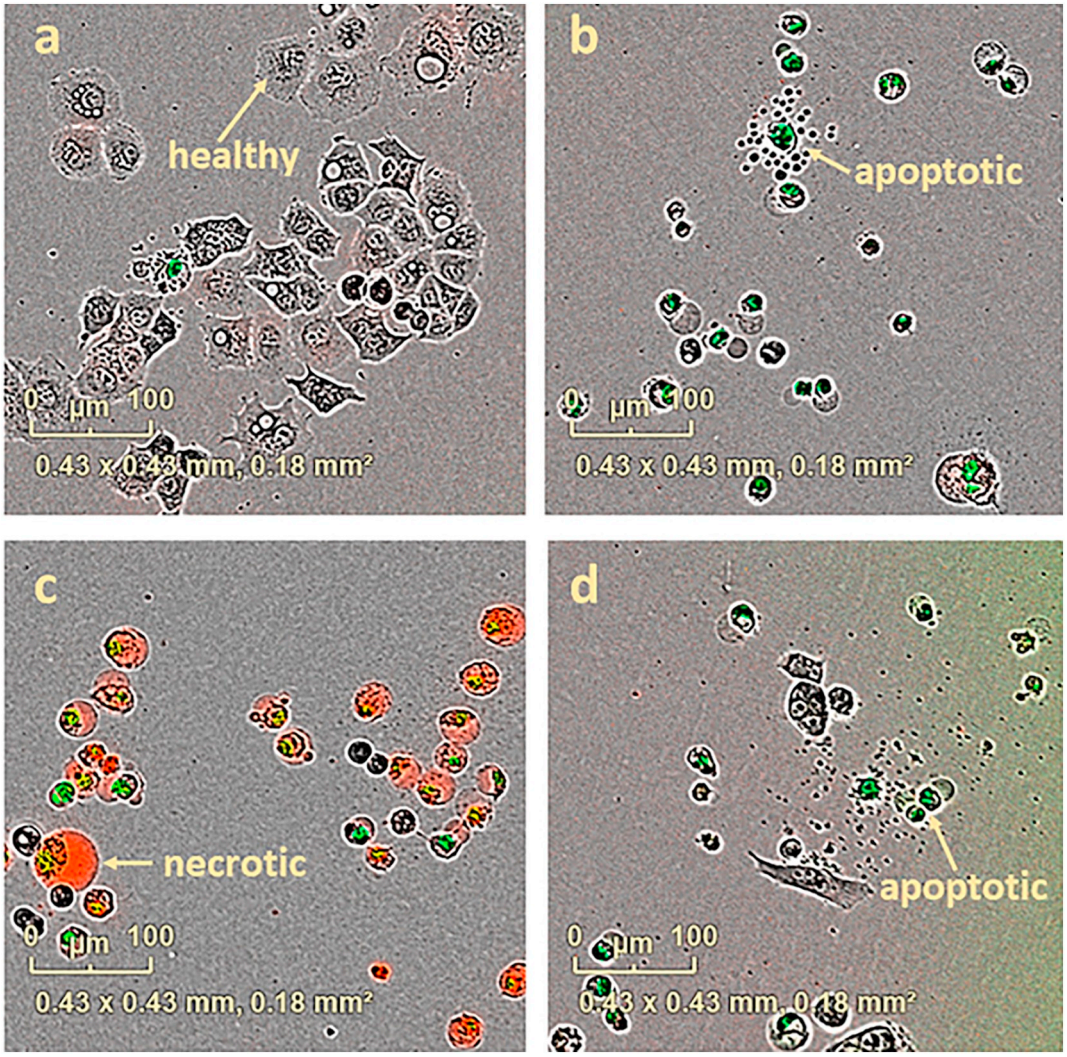

Fig. 4. Typical morphology and fluorescent staining of PANC-1 cells (IncuCyte Zoom with ×10 objective; blended phase contrast and green and red fluorescence channels) [37] under the treatment conditions listed in Table 2: (a) condition 1, 48 h; (b) condition 2, 48 h; (c) condition 4, 4 h; and (d) condition 6, 48 h. Caspase 3/7 green stain for apoptosis (3.0 µM) [41] and Cytotox Red stain for dead cells (0.30 µM) [42] were added to cell culture medium (see Experimental Section). Typical healthy, apoptotic (green staining, apoptotic bodies) [52] and necrotic (red staining, membrane blebbing) [53,54] cells are marked by arrows. Green fluorescence intensity has been enhanced for better visibility. Full-scale phase contrast and fluorescence images corresponding to (a–d) with original fluorescence intensities are shown in Fig. S5. (For interpretation of the references to color in this figure legend, the reader is referred to the web version of this article.)

3.5. Decomposition of **2** and **2**-HSA in cell culture medium

Results of UV–vis spectroscopic studies of the reactions of **2** and its derivatives (conditions 2–8 in Table 2; 10 µM V) with cell culture medium at 310 K are shown in Fig. S5, Supplementary Information. The medium used in these experiments was identical to that used in cell assays, except that it did not contain phenol red, and was additionally supplemented with 10 mM HEPES (4-(2-hydroxyethyl)-1-piperazineethanesulfonic acid) to maintain a pH value of 7.4 under an ambient atmosphere [14]. Absorbance peaks due to V-dtbc species (λ_{max} = 660 or 390 nm, Fig. 3a) were observed immediately after the addition of fresh or decomposed solutions of **2** in DMF to cell culture medium (Fig. S4). These peaks mostly disappeared after 24 h at 310 K, leading to featureless spectra over 300–820 nm that were similar at all conditions, except for trace absorbance at 660 nm for condition 3 (Table 2). The data within Fig. S5 support the choice of equilibration conditions of **2** and its derivatives with cell culture medium prior to cell treatment (24 h at 310 K; 3, 5, 7–10 in Table 2).

3.6. Real-time cell proliferation and cytotoxicity assays

Real-time cell proliferation assays using an IncuCyte Zoom imaging system [37] provided deeper insight into the mechanism of anti-cancer activity of **2** and its derivatives, compared with the commonly used endpoint assays [51]. Quantitative real-time cytotoxicity measurements were performed with fluorescent dyes that were specifically designed for IncuCyte: green-fluorescent Caspase 3/7 reagent (specific for early stage apoptosis) [41] and red-fluorescent Cytotox reagent (staining late apoptotic and necrotic cells with damaged membranes) [42]. Typical morphological features [52–54] and fluorescent staining of healthy, apoptotic and necrotic PANC-1 cells are shown in Fig. 4, and the corresponding full-scale phase contrast and fluorescence images are shown in Fig. S6, Supplementary Information.

Typical time-dependent changes in cell proliferation (phase contrast images), apoptosis (green fluorescence) and cell death (red fluorescence) under the conditions of Table 2 (10 µM V) are shown in Fig. 5 and in Fig. S7, Supplementary Information. All the V-containing treatments (2–9 in Table 2) caused > 50% inhibition of PANC-1 cell proliferation at 72 h at 10 µM V (Figs. 5a and S6a, b), which was higher

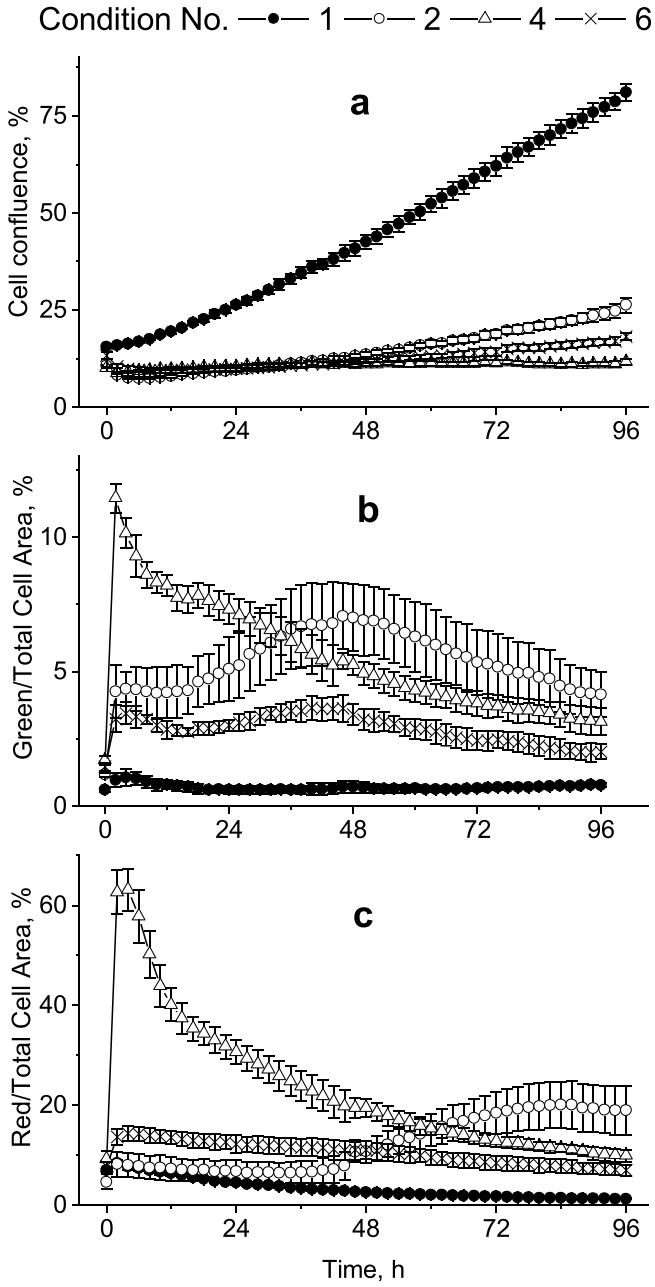

Fig. 5. Time dependences of cell proliferation (a; phase contrast images), apoptosis (b; green fluorescence, Caspase 3/7 stain) [41] and necrosis/cell death (c; red fluorescence, Cytotox Red stain) [42] for selected treatment conditions (Table 2), as observed by IncuCyte Zoom imaging system [37]. Error bars represent the mean values and standard deviations for six replicate wells. The corresponding data for the all the conditions listed in Table 2 are given in Fig. S6, Supporting Information.

than expected based on the IC_{50} values in Table 2. This increase in anti-proliferative activity is likely to be caused by photo-activation of V species [55] with the laser light (λ_{ex} = 488 nm) used in IncuCyte experiments [37]. However, the extent of cell proliferation inhibition under various conditions (4 > 6 > 2–3–5–7–8 > 9 > 10; Figs. 5a and S7a,b) corresponded to the order of IC_{50} values listed in Table 2.

In agreement with the results of cell viability assays (condition 4 in Table 2 and Fig. S4), an aged solution of **2** in DMF that was freshly added to cell culture medium (10 μM V) completely halted cell proliferation immediately after the treatment (condition 4 in Fig. 5a). These conditions also caused remarkably rapid (2–4 h after the treatment) and extensive onset of cell necrosis (condition 4 in Fig. 5c), which was characterized by red fluorescence staining and membrane blebbing in the affected cells (Figs. 4c and S6c) [53,54]. There was also concomitant significant increase in cell apoptosis (condition 4 in Fig. 5b, and green fluorescent cells in Fig. S5c). Fresh solutions of **2** in DMF that were freshly added to cell culture medium caused slower and less extensive onset of apoptosis and cell death, which peaked at ~48 h and ~80 h, respectively (condition 2 in Fig. 5b, c). Notably, a fresh **2**-HSA adduct caused stronger inhibition of cell proliferation, but a lower extent of apoptosis and cell death, compared with a fresh solution of **2** in DMF (conditions 2 and 6 in Table 2 and in Fig. 5). Typical apoptotic cells, featuring green fluorescence and apoptotic bodies [52], were observed under both conditions (Fig. 4b, d).

Conditions 3, 5 and 7 in Table 2 (decomposition products of **2** or **2**-HSA in cell culture medium, 10 μM V) led to a similar degree of inhibition in cell proliferation (~60% at 72 h, Fig. S7a), but the time profiles of apoptosis and cell death were different (Fig. S7c, e), which indicated that the decomposition products formed under these conditions were not the same. For instance, the extent of apoptosis caused by the decomposition products of **2**-HSA (condition 7) was the lowest among all the V-containing treatments (Figs. 5b and S7c, d). Taken together, the data within Figs. 5 and S6 suggest that the action of **2**-HSA adduct on PANC-1 cells was predominantly anti-proliferative, while the solutions of **2** in DMF led to significant cell death via apoptosis and/or necrosis, particularly after aging. Time-dependent cell proliferation and cytotoxicity studies (Figs. 5 and S7) highlighted the crucial role of speciation of V complexes in cell culture medium and in stock solutions in their activity in cell-based assays [13–15,56].

*3.7. Mechanisms of anti-proliferative and cytotoxic activity of **2** and implications for anti-cancer treatment*

Like the previously studied V(V)-Schiff base-catecholato complex, **1** [21], strong absorbance in the visible range (Fig. 3a) due to charge transfer between the V(V) center and catecholato ligands [22] facilitated stability studies of **2** under cell culture conditions. Complex **2** persisted longer than **1** under the conditions of cell assays, since trace absorbance at λ_{max} = 660 nm was observed even after 24 h of reaction of **2** (10 μM) with cell culture medium at 310 K (Fig. S5a, f), while **1** decomposed completely under these conditions [21]. On the other hand, **1** was relatively stable in stock solutions (10 mM in DMF or DMSO) that were used for cell assays [21], while **2** decomposed visibly within days under ambient conditions (Figs. 2a and S2). Spectral changes in DMF solutions within 1–3 d at 298 K were also reported for **3** [31], although the reaction mechanism has not been examined.

The main decomposition pathway of **2** in organic solvents, based on literature data on V(V)-catalyzed oxidation of $dtbcH_2$ by O_2 [28,29] and on the ESI-MS results (Fig. 2e, f and Table 1), is shown in Scheme 1a. Interestingly, the decomposition products of **2** in organic solvents were much more cytotoxic than the fresh complex **2** (conditions 2 and 4 in Table 2 and Fig. 5), while the opposite trend was observed for **3** [31]. Thus, unlike for **1** [21], the cytotoxicity of **2** was not due to cellular uptake of the intact complex. The most likely reactive species in this case were $[VO(dtbc)_2]^-$ or similar V(V)-oxido-catecholato complexes (framed in Scheme 1) [30], based on the absence of other potential reactive species (V(IV) complexes or semiquinone radicals) [27,44] in EPR spectra of decomposed solutions of **2** (Fig. S3). Other evidence that the decomposition products of **2**, such as $[VO(dtbc)_2]^-$, are the likely ultimate cytotoxic species, is the delayed onset of apoptosis and cell death when fresh solution of **2** in DMF is directly added to cell culture medium, compared with rapid effect of the aged solution of **2** in DMF (conditions 2 and 4 in Fig. 5b, c).

Formation of $[VO(dtbc)_2]^-$ and other reactive V(V) species [30] after the addition of **2** to cell culture medium (Scheme 1b) explains the similar anti-proliferative and cytotoxic effects of **2** before and after its equilibration with cell culture medium (conditions 2 and 3 in Table 2

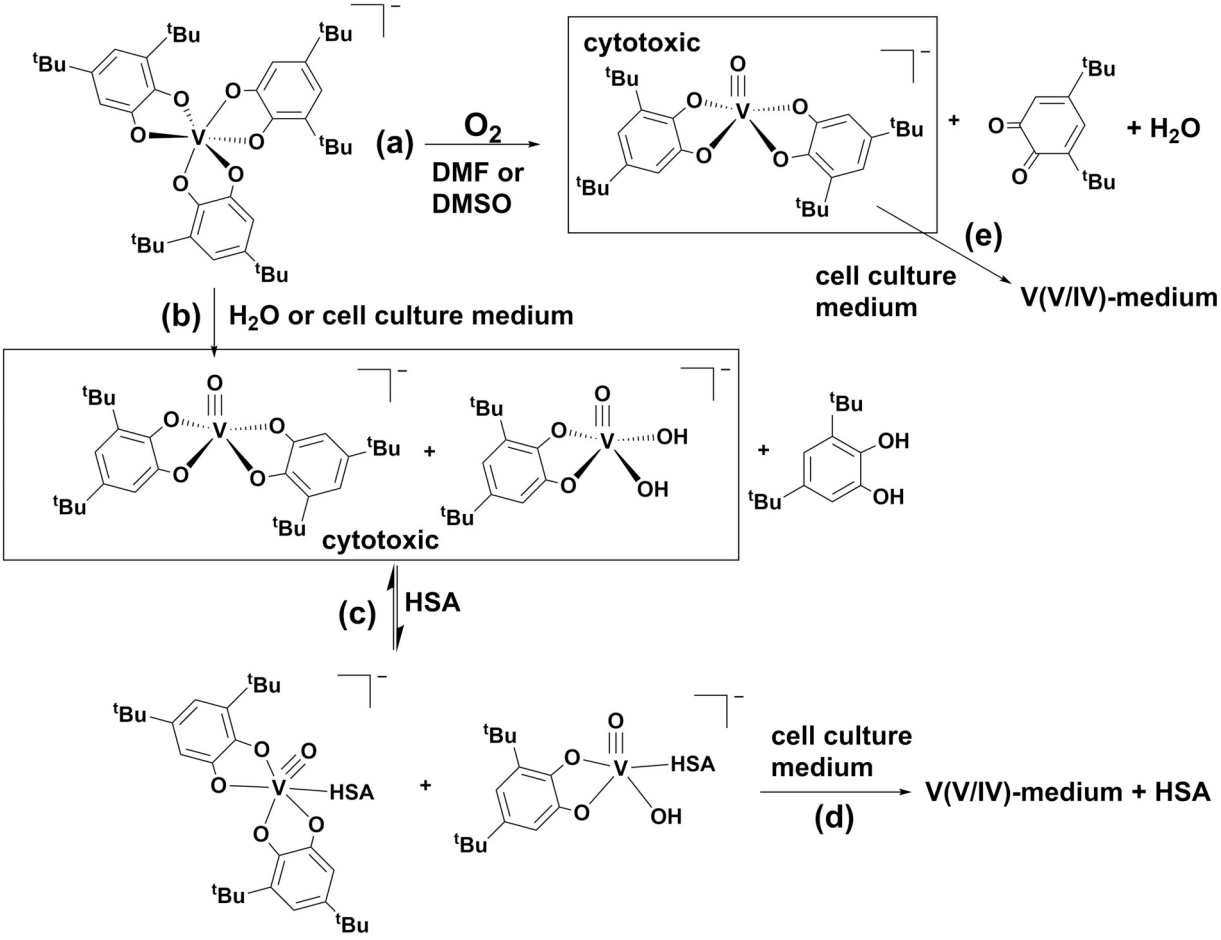

Scheme 1. Proposed reactivity pathways (a–e) of **2** in aqueous and organic solvents under the conditions of cell assays (HSA is human serum albumin). The likely cytotoxic species are designated by framing.

and in Figs. 5 and S7), in contrast to the drastic decrease in activity observed for **1** [21]. This factor is likely to complicate the use of **2** for direct injection into pancreatic and other cancer tumors [7,8], since cytotoxic decomposition products of the drug will lead to high systemic toxicity. However, this disadvantage can be overcome by using appropriate formulations of **2**, such as **2**-HSA adducts. Addition of **2** to aqueous solution of HSA is likely to lead to the formation of V(V)-HSA adducts that partially retain bound catecholato ligands (Scheme 1c), similarly to the extensively studied reactions of anti-diabetic V(IV) complexes with blood serum proteins [57–59]. Comparison of conditions 6 and 7 in Table 1 and in Figs. 5b and S6 shows that the decomposition of **2**-HSA adducts in cell culture medium (Scheme 1d) [49] supressed the induction of apoptosis at ~48 h of treatment and significantly reduced the anti-proliferative activity of **2**-HSA. Similarly, the anti-proliferative and cytotoxic activity of an aged solution of **2** in DMF drastically decreased after its equilibration with cell culture medium (conditions 4 and 5 in Table 2 and in Figs. 5 and S7), as shown in Scheme 1e.

The adduct with HSA is also a convenient delivery form of **2**, since it is stable in the dry form, and can be dissolved in physiological saline immediately before use. The use of HSA as a delivery vehicle for anti-cancer drugs has become increasingly common, because HSA stabilizes lipophilic drugs in aqueous solutions and facilitates their uptake by cancer cells [48]. A recent precedent for metal-based drugs is a non-covalent HSA adduct of a lipophilic Pt(IV) pro-drug that is converted to cytotoxic Pt(II) species in the reducing environment of solid tumors [47]. Formation of albumin adduct of a Ru(III) complex, NAMI-A, is likely to be responsible for its anti-metastatic activity [60]. Optimization of conditions for the preparation of HSA adducts with **2** or other lipophilic V(V) and V(IV) complexes, such as **1** [21] or **3** [31], can lead to the development of clinically useful formulations for treating pancreatic cancer and other difficult-to-treat cancers by intratumoral injections (A. Levina, D. C. Crans, P. A. Lay et al., manuscript in preparation).

4. Conclusions

A stable non-oxido V(V) complex, $(NH_4)[V(dtbc)_3]$ (**2**; $dtbcH_2$ = 3,5-di-*tert*-butylcatechol) [22,24] was synthesized conveniently in high yield by the reaction of NH_4VO_3 with three equivalents of $dtbcH_2$ in MeCN under ambient conditions. The complex underwent redox reactions in polar organic solvents (DMF or DMSO) in the presence of O_2 (Scheme 1a), which led to the formation of reactive V(V) oxido-catecholato intermediates, such as $[VO(dtbc)_2]^-$ (detected by ESI-MS, Fig. 2 and Table 1). These intermediates were likely to be responsible for the rapid onset of cell death via necrotic pathway when aged stock solutions of **2** in DMF were used for cell culture assays (condition 4 in Table 2). The same intermediates were formed to a lesser extent when freshly prepared stock solutions of **2** were added to cell culture medium (condition 2 in Table 2). The extensive reactivity of **2** in both organic and aqueous media (Scheme 1) complicates its use for controlled anti-cancer activity. One possibility to avoid such complications is the isolation of adducts of **2** with human serum albumin (HSA). Although **2** was likely to partially lose the catecholato ligands during the binding to HSA in aqueous solutions, the resultant adduct showed strong anti-proliferative activity in PANC-1 cells with no

significant necrotic cell death (condition 6 in Table 2 and Fig. 5). The effect of **2**-HSA adduct was reduced after the decomposition in cell culture medium for 24 h at 310 K (condition 7 in Table 2 and Fig. S6), which is likely to lead to the loss of remaining catecholato ligands and to binding of the resultant V(V/IV) oxido species to the medium components [14]. These properties make the **2**-HSA adduct a suitable candidate for potential use in intratumoral injection formulations for the treatment of pancreatic cancer [7,8].

Declaration of competing interest

The authors have no conflict of interest to disclose.

Acknowledgments

Financial support for this work was provided by Australian Research Council (ARC) Discovery grants to PAL for an ARC Senior Research Associate position for AL (DP130103566, DP160104172) and Linkage Infrastructure and Equipment Facility grant LE for the EPR instrument. The authors acknowledge the facilities and the scientific and technical assistance of the Australian Microscopy & Microanalysis Research Facility at the Australian Centre for Microscopy & Microanalysis at the University of Sydney (Drs Minh Huynh and Ellie Kable) for the use of cell culture laboratory, Molecular Biology Facility of the Bosch Institute, University of Sydney (Drs Donna Lai and Sheng Hua) for the use of IncuCyte Zoom, and Sydney Analytical for the EPR spectroscopic measurements. We thank Dr. Nicholas Proschogo and Mr. Tim Katte (University of Sydney) for performing high-resolution ESI-MS measurements.

Appendix A. Supplementary data

Figures showing the high-resolution ESI-MS data for **2** (Fig. S1); the time-dependent changes in UV–vis spectra of **2** in organic solvents (Fig. S2); EPR spectra of decomposed solution of **2** in DMF in comparison with that of aqueous V(IV) (Fig. S3); results of WST-8 viability assays of **2** and its decomposition products in PANC-1 cells (Fig. S4); UV–vis spectra of **2** and its decomposition products (10μM V) in cell culture medium (Fig. S5); typical phase contrast and fluorescence images of PANC-1 cells treated with fresh and decomposed **2** and with **2**-HSA adduct (Fig. S6); and kinetics of cell proliferation, apoptosis and cell death for PANC-1 cells treated with decomposition products of **2** (Fig. S7). Supplementary data to this article can be found online at https://doi.org/10.1016/j.jinorgbio.2019.110815.

References

[1] G. Barr-David, T.W. Hambley, J.A. Irwin, R.J. Judd, P.A. Lay, B.D. Martin, R. Bramley, N.E. Dixon, P. Hendry, J.-Y. Ji, R.S.U. Baker, A.M. Bonin, Inorg. Chem. 31 (1992) 4906–4908.
[2] J.C. Pessoa, S. Etcheverry, D. Gambino, Coord. Chem. Rev. 301-302 (2015) 24–48.
[3] D. Rehder, Future Med. Chem. 8 (2016) 325–338.
[4] D.C. Crans, L. Yang, A. Haase, X. Yang, Met. Ions Life Sci. 18 (2018) 251–280.
[5] M. Selman, C. Rousso, A. Bergeron, H.H. Son, R. Krishnan, N.A. El-Sayes, O. Varette, A. Chen, F. Le Boeuf, F. Tzelepis, J.C. Bell, D.C. Crans, J.-S. Diallo, Mol. Ther. 26 (2018) 56–69.
[6] D.C. Crans, H. LaRee, G. Cardiff, G. Posner, Met. Ions Life Sci. 19 (2019), https://doi.org/10.1515/9783110527872-014.
[7] K. Takakura, S. Koido, World J. Clin. Oncol. 6 (2015) 216–219.
[8] Y. Hirooka, H. Kasuya, I.B. Villalobos, Y. Naoe, T. Ichinose, T. Ishikawa, H. Kawashima, E. Ohno, H. Goto, N. Koyama, M. Tanaka, Y. Kodera, BMC Cancer 18 (2018) 596.
[9] S. Kowalski, I. Inkielewicz-Stepniak, S. Hac, D. Wyrzykowski, A. Zauszkiewicz-Pawlak, Oncotarget 8 (2017) 60324–60341.
[10] S. Kowalski, I. Inkielewicz-Stepniak, D. Wyrzykowski, S. Hac, M. Rychlowski, M.W. Radomski, Int. J. Mol. Sci. 20 (2019) E261.
[11] D.C. Crans, J.J. Smee, E. Gaidamauskas, L. Yang, Chem. Rev. 104 (2004) 849–902.
[12] D.C. Crans, Pure Appl. Chem. 77 (2005) 1497–1527.
[13] D.C. Crans, K.A. Woll, K. Prusinskas, M.D. Johnson, E. Norkus, Inorg. Chem. 52 (2013) 12262–12275.
[14] A. Levina, D.C. Crans, P.A. Lay, Coord. Chem. Rev. 352 (2017) 473–498.
[15] A. Levina, P.A. Lay, Chem. Asian J. 12 (2017) 1692–1699.
[16] K.H. Thompson, C. Orvig, J. Inorg. Biochem. 100 (2006) 1925–1935.
[17] K.H. Thompson, J. Lichter, C. LeBel, M.C. Scaife, J.H. McNeill, C. Orvig, J. Inorg. Biochem. 103 (2009) 554–558.
[18] G.R. Willsky, K. Halvorsen, M.E. Godzala, III, L.-H. Chi, M.J. Most, P. Kaszynski, D.C. Crans, A.B. Goldfine, P.J. Kostyniak, Metallomics 5 (2013) 1491–1502.
[19] S. Trevino, A. Diaz, E. Sanchez-Lara, B.L. Sanchez-Gaytan, J.M. Perez-Aguilar, E. Gonzalez-Vergara, Biol. Trace Elem. Res. 188 (2019) 68–98.
[20] D.C. Crans, J.T. Koehn, S.M. Petry, C.M. Glover, A. Wijetunga, R. Kaur, A. Levina, P.A. Lay, Dalton Trans. 48 (2019) 6383–6395.
[21] C.R. Cornman, G.J. Colpas, J.D. Hoeschele, J. Kampf, V.L. Pecoraro, J. Am. Chem. Soc. 114 (1992) 9925–9933.
[22] C. Milsmann, A. Levina, H.H. Harris, G.J. Foran, P. Turner, P.A. Lay, Inorg. Chem. 45 (2006) 4743–4754.
[23] S.R. Cooper, Y.B. Koh, K.N. Raymond, J. Am. Chem. Soc. 104 (1982) 5092–5102.
[24] M.E. Cass, N.R. Gordon, C.G. Pierpont, Inorg. Chem. 25 (1986) 3962–3967.
[25] C.J. Leggett, B.F. Parker, S.J. Teat, Z. Zhang, P.D. Dau, W.W. Lukens, S.M. Peterson, A.J.P. Cardenas, M.G. Warner, J.K. Gibson, J. Arnold, L. Rao, Chem. Sci. 7 (2016) 2775–2786.
[26] J.-A. Yan, Y.-S. Chen, Y.-H. Chang, C.-Y. Tsai, C.-L. Lyu, C.-G. Luo, G.-H. Lee, H.-F. Hsu, Inorg. Chem. 56 (2017) 9055–9063.
[27] M. Domarus, M.L. Kuznetsov, J. Marcalo, A.J.L. Pombeiro, J.A.L. da Silva, Angew. Chem. Int. Ed. 55 (2016) 1489–1492.
[28] C.-X. Yin, R.G. Finke, J. Am. Chem. Soc. 127 (2005) 9003–9013.
[29] C.-X. Yin, R.G. Finke, J. Am. Chem. Soc. 127 (2005) 13988–13996.
[30] Y. Yoshikawa, H. Sakurai, D.C. Crans, G. Micera, E. Garribba, Dalton Trans. 43 (2014) 6965–6972.
[31] K. Dankhoff, A. Ahmad, B. Weber, B. Biersack, R. Schobert, J. Inorg. Biochem. 194 (2019) 1–6.
[32] L.G. Naso, L. Lezama, M. Valcarcel, C. Salado, P. Villace, D. Kortazar, E.G. Ferrer, P.A.M. Williams, J. Inorg. Biochem. 157 (2016) 80–93.
[33] J.J. Martinez Medina, E.G. Ferrer, P.A.M. Williams, N.B. Okulik, Inorg. Chim. Acta 487 (2019) 369–378.
[34] D. Rehder, T. Polenova, M. Bühl, Annu. Rep. NMR Spectrosc. 62 (2007) 49–114.
[35] H.E. Gottlieb, V. Kotlyar, A. Nudelman, J. Org. Chem. 62 (1997) 7512–7515.
[36] M. Senko, IsoPro 3.0, Sunnyvale, CA, USA, (1998).
[37] Essen Bioscience, IncuCyte Zoom 2015 Live Cell Imaging System and Data Processing Software, www.essenbioscience.com, 2015.
[38] Dojindo Molecular Technologies, Cell Counting Kit 8, http://www.dojindo.com/store/p/456-Cell-Counting-Kit-8, 2017.
[39] Microcal Software Inc, Microcal Origin 6.1, Northampton, MA, USA, (1999).
[40] R.I. Freshney, Culture of Animal Cells: A Manual of Basic Technique and Specialized Applications, 7th edition, Wiley-Blackwell, Hoboken, NJ, USA, 2016.
[41] Essen Bioscience, IncuCyte Caspase-3/7 Reagent for Apoptosis. Cat. No. 4440. Product Data Sheet, www.essenbioscience.com, 2018.
[42] Essen Bioscience, IncuCute Cytotox Red Reagent for Counting Dead Cells. Cat. No. 4633. Product Data Sheet. www.essenbioscience.com, 2018.
[43] A. Butler, R. De la Rosa, Q. Zhou, A. Jhanji, C.J. Carrano, Inorg. Chem. 31 (1992) 5072–5077.
[44] H. Preiss, D. Schultze, K. Szulzewsky, J. Eur. Ceram. Soc. 19 (1998) 187–194.
[45] M. Le, O. Rathje, A. Levina, P.A. Lay, J. Biol. Inorg. Chem. 22 (2017) 663–672.
[46] T.S. Smith, R. LoBrutto, V.L. Pecoraro, Coord. Chem. Rev. 228 (2002) 1–18.
[47] Y.-R. Zheng, K. Suntharalingam, T.C. Johnstone, H. Yoo, W. Lin, J.G. Brooks, S.J. Lippard, J. Am. Chem. Soc. 136 (2014) 8790–8798.
[48] E.N. Hoogenboezem, C.L. Duvall, Adv. Drug Deliv. Rev. 130 (2018) 73–89.
[49] A. Levina, A.I. McLeod, A. Pulte, J.B. Aitken, P.A. Lay, Inorg. Chem. 54 (2015) 6707–6718.
[50] M. Timm, L. Saaby, L. Moesby, E.W. Hansen, Cytotechnology 65 (2013) 887–894.
[51] M. Niepel, M. Hafner, M. Chung, P.K. Sorger, Curr. Protoc. Chem. Biol. 9 (2017) 55–74.
[52] A. Saraste, K. Pulkki, Cardiovasc. Res. 45 (2000) 528–537.
[53] U. Ziegler, P. Groscurth, News Physiol. Sci. 19 (2004) 124–128.
[54] R. Andrade, L. Crisol, R. Prado, M.D. Boyano, J. Arluzea, J. Arechaga, Biol. Cell. 102 (2010) 25–35.
[55] U. Schatzschneider, Eur. J. Inorg. Chem. (2010) 1451–1467.
[56] K.A. Doucette, K.N. Hassell, D.C. Crans, J. Inorg. Biochem. 165 (2016) 56–70.
[57] D. Sanna, G. Micera, E. Garribba, Inorg. Chem. 52 (2013) 11975–11985.
[58] J. Costa Pessoa, G. Goncalves, S. Roy, I. Correia, S. Mehtab, M.F.A. Santos, T. Santos-Silva, Inorg. Chim. Acta 420 (2014) 60–68.
[59] I. Correia, I. Chorna, I. Cavaco, S. Roy, M.L. Kuznetsov, N. Ribeiro, G. Justino, F. Marques, T. Santos-Silva, M.F.A. Santos, H.M. Santos, J.L. Capelo, J. Doutch, J.C. Pessoa, Chem. Asian J. 12 (2017) 2062–2084.
[60] M. Liu, Z.J. Lim, Y.Y. Gwee, A. Levina, P.A. Lay, Angew. Chem. Int. Ed. 49 (2010) 1661–1664.